journal

J. Am. Ceram. Soc., 91 [5] 1475–1480 (2008)
DOI: 10.1111/j.1551-2916.2008.02319.x

Thermochemical and Mechanical Stabilities of the Oxide Scale of ZrB_2+SiC and Oxygen Transport Mechanisms

Ju Li and Thomas J. Lenosky†

Department of Materials Science and Engineering, University of Pennsylvania, Philadelphia, Pennsylvania 19104

Clemens J. Först and Sidney Yip

Department of Nuclear Science and Engineering and Department of Materials Science and Engineering, Massachusetts Institute of Technology, Cambridge, Massachusetts 02139

Refractory diboride with silicon carbide additive has a unique oxide scale microstructure with two condensed oxide phases (solid+liquid), and demonstrates oxidation resistance superior to either monolithic diboride or silicon carbide. We rationalize that this is because the silica-rich liquid phase can retreat outward to remove the high SiO gas volatility region, while still holding onto the zirconia skeleton mechanically by capillary forces, to form a "solid pillars, liquid roof" scale architecture and maintain barrier function. Basic assessment of the oxygen carriers in the borosilicate liquid in oxygen-rich condition is performed using first-principles calculations. It is estimated from entropy and mobility arguments that above a critical temperature $T_C \sim 1500°C$, the dominant oxygen carriers should be network defects, such as peroxyl linkage or oxygen-deficient centers, instead of molecular O_2^* as in the Deal–Grove model. These network defects will lead to sublinear dependence of the oxidation rate with external oxygen partial pressure. The present work suggests that there could be significant room in improving the high-temperature oxidation resistance by refining the oxide scale microstructure as well as controlling the glass chemistry.

I. Introduction

Refractory diborides (HfB_2, ZrB_2) with 20–30 vol% SiC additive are prominent ultrahigh-temperature ceramics withstanding temperatures 2000 K and above.[1,2] During operation in air its surface is oxidized, giving rise to a crystalline oxide skeleton (HfO_2, ZrO_2) and a silica-rich borosilicate liquid that wets it,[3–10] produced by the reactions:

$$ZrB_2(c) + (5/2)O_2 \rightarrow ZrO_2(c) + B_2O_3(l,g) \quad (1)$$

$$SiC(c) + (3/2)O_2 \rightarrow SiO_2(l) + CO(g) \quad (2)$$

respectively. Intense research is ongoing to characterize and enhance this scale as a barrier against oxygen[11–23] (the scale microstructure can be seen in, for example, Fig. 4 of Opila *et al.*[15]), which apparently is superior to that of either monolithic diboride or SiC at the intended high temperatures (see Fig. 1).

The reason for the first superiority (ZrB_2+SiC > ZrB_2) is well understood. Pure B_2O_3 melts at 450°C and evaporates rather quickly above 1100°C. In contrast, SiO_2 is a strong network former (pure SiO_2 has a glass transition temperature of 1175°C), with much larger viscosity as well as much smaller equilibrium vapor pressure than B_2O_3 (see Figs. 15 and 16 of Monteverde and Bellosi).[12,13] Thus, oxygen diffusion should be more sluggish in the silica-rich liquid than in pure B_2O_3 (*l*), which furthermore will be evaporating rather quickly above 1100°C.

The reason for the second superiority (ZrB_2+SiC > SiC) is less well understood. The crystalline oxide phase $ZrO_2(c)$ formed is often highly porous—although in arc jet testing above 2000 K it appears that $ZrO_2(c)$ could sinter into a less porous compact layer,[16,17] thereby potentially becoming protective also. Whether the *in situ* formed $ZrO_2(c)$, when fully dense, is as a significant barrier to oxygen diffusion as SiO_2 (*l*) in open-circuit condition, is an interesting question that depends on its electronic conductivity, which in turn depends on how the charge defects are compensated inside the crystal, related to the amount of impurities. Irrespective of the outcome of that discussion, however, if $ZrO_2(c)$ is quite porous its barrier function is lost, because gas-phase diffusion through the percolating cracks and pores, even in the Knudsen diffusion regime, is much easier than diffusion in condensed phases. In that case then, properties of the silica-rich liquid will control the effective barrier function of the scale, because it flows to fill in the cracks and pores of $ZrO_2(c)$, as well as forming an overlayer on top (a "liquid roof," see for instance Fig. 4 of Opila *et al.*[15] and Fig. 6 of Rezaie *et al.*[22]), thus occupying both parallel and serial oxygen transport routes.

We suggest an explanation for the second superiority (ZrB_2+SiC > SiC) in Section II, based on the notion that a protective condensed-phase oxide scale must be stable both thermochemically and mechanically, even when the volatility diagram[2,21,24,25] predicts high vapor pressures (>1 atm = 101 325 Pa) in certain regions of the scale. We think the experiments[15,16,21,22] suggest that with a porous $ZrO_2(c)$ skeleton, the high gas volatility problem can be avoided simply by the liquid phase retreating somewhat outwards,[21] while still maintaining mechanical integrity by holding onto the outer $ZrO_2(c)$ skeleton with capillary forces. The porous $ZrO_2(c)$ skeleton acts as a condensing substrate and mechanical support to the borosilicate liquid. This is not available when oxidizing monolithic SiC, where the SiO_2 (*l*) is mechanically unstable against gas bubble coalescence and layer shear-off or spallation above the SiO boiling temperature.

In Section III, we make some molecular-level predictions regarding likely oxygen transport mechanisms in the borosilicate liquid, based on density functional theory (DFT) calculations. While it is commonly accepted that molecular O_2 permeate through the glassy network at low temperatures,[26] the DFT calculation results suggest that network incorp orated defects such as peroxyl linkage[27,28] or oxygen-deficient centers[29,30] will overtake molecular O_2 as dominant oxygen carriers at above ~1500°C.

Y. Blum—contributing editor

Manuscript No. 23766. Received September 19, 2007; approved December 12, 2007.
This work was performed mostly at the Ohio State University and supported by the Ceramics and Non-Metallic Materials Program in the Air Force Office of Scientific Research (FA9550-05-1-0026).
Presented at the AFOSR Workshop on Ultra-High-Temperature Ceramic Materials hosted by SRI International, July 23–25, 2007.
†Author to whom correspondence should be addressed. e-mail liju99@alum.mit.edu

II. Thermochemical and Mechanical Stability Analysis of the Oxide Scale

ZrB_2+SiC has a complex scale structure containing at least two condensed phases: $ZrO_2(c)$, which in this section is assumed to be a highly porous skeleton with percolating holes, and a silica-rich liquid phase that wets the skeleton. Gas species of the greatest interest are B_2O_3, SiO, and CO, although BO, B_2O_2, B_2O, etc. are also present and can be the dominant gas carriers in reducing conditions, and can play important roles in mass transport.[31] SiO could evolve by for instance:

$$2SiO_2(l) \rightarrow 2SiO(g) + O_2 \quad (3)$$

(3) is a key reaction that has been used in constructing vola tility diagrams.[2,21,24,25] When *in contact* with $SiO_2(l)$, with decreasing oxygen chemical potential or the equivalent partial pressure ($pO_2\downarrow$), SiO will have higher equilibrium vapor pressure ($pSiO\uparrow$). Volatility diagram of the ZrB_2+SiC system[2,21] indicates that when $T > T_B \approx 1775°C$, the peak equilibrium vapor pressure of SiO inside the scale could exceed 1 atm, which would then induce a boiling transition (gas bubbles can nucleate and grow inside the liquid). This violently disrupts the $SiO_2(l)$ scale in the case of oxidizing monolithic SiC. However, the scales of ZrB_2+SiC and HfB_2+SiC appear to be much more tolerant of such a boiling transition. It is precisely in this $T > T_B$ regime that ZrB_2+SiC and HfB_2+SiC demonstrate oxidation resistance superior to monolithic SiC, which otherwise is considered a highly oxidation-resistant material (see Fig. 1).

We hereby suggest a "dynamic view" (Fig. 2(a)) and a "steady-state view" (Fig. 2(b)) of why ZrB_2+SiC is superior to monolithic SiC. The two views are inherently consistent. Imagine a ZrB_2+SiC specimen is gradually being heated up in an oxygen-rich environment like normal air ($pO_2 = 0.2$ atm), initially from $T \ll T_B$. At such high ambient pO_2, a protective $SiO_2(l)$ film will condense on top from the very beginning,[24] that wets the $ZrO_2(c)$ skeleton, leaving no voids at the base. At $T < T_B$, monolithic SiC in fact resist oxidation better than ZrB_2+SiC. Also at $T < T_B$, the $pSiO$ branch of the volatility diagram[2,21] in contact with $SiO_2(l)$ has a formal thermodynamic definition but is not physically realizable as pure SiO gas bubbles, because any SiO gas bubble anywhere will be crushed by the dual forces of surface tension and hydrostatic pressure, which we take to be 1 atm inside $SiO_2(l)$. However, as the temperature is brought up to $T > T_B$, a sharp transition happens inside $SiO_2(l)$. Now SiO gas bubbles can nucleate at the base, with $\Delta p \equiv pSiO - 1\ \text{atm} > 0$ working against the surface tension. The dynamic view (Fig. 2(a)) examines how the gas bubbles grow and coalesce, paying attention to the role of the $ZrO_2(c)$ skeleton.

It is likely that the $ZrO_2(c)$ skeleton will regulate gas bubble dynamics. Unlike unconstrained growth inside a completely

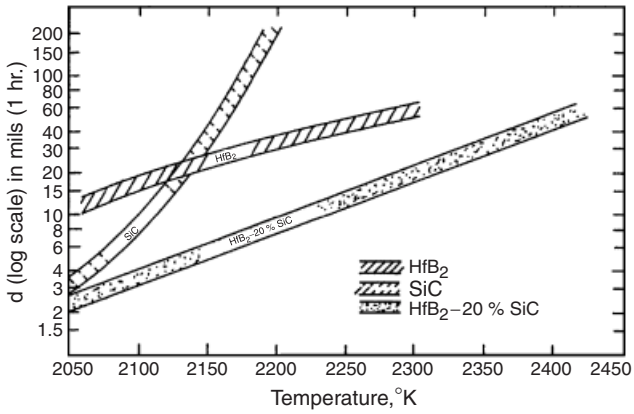

Fig. 1. One-hour oxidation resistance of monolithic HfB_2, monolithic SiC, and HfB_2+SiC composite (taken from Clougherty, Pober, and Kaufman).[7]

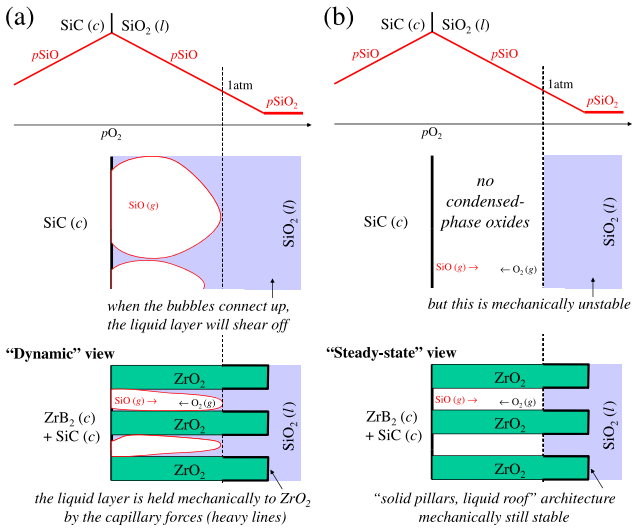

Fig. 2. The "dynamic view" (a) and "steady-state view" (b) of why ZrB_2+SiC has better oxidation resistance than monolithic SiC above the SiO boiling transition temperature.

liquid scale, gas bubbles (SiO, CO, B_2O_3, BO, O_2, etc. mixture) in a semisolid porous scale are forced to grow into long fingers (a pressure difference of the order atm is large enough to displace a liquid, but usually not enough to displace a solid). Reaction (3) could then happen on one end of the gas finger, BO, B_2O_3, SiO, CO, etc. would then diffuse along the gas finger with O_2 diffusing in the opposite direction, and finally when pO_2 gets high enough, SiO could get reoxidized to form $SiO_2(l)$ on the other end of the finger,[22] and B_2O_3, etc. would get solvated in the liquid and continue to diffuse up the scale. This is equivalent to a channeling transfer of $SiO_2(l)$ from one end of the finger to the other, which is mechanically untenable without the support and constraint of the $ZrO_2(c)$ skeleton. In reality the pores are tortuous instead of straight, giving the effusing $SiO(g)$ much opportunity to react with $O_2(g)$ near the end, and the $SiO_2(l)$ product collected on the $ZrO_2(c)$ substrate. The skeleton may also impart significant mechanical integrity to the scale in the case of bubble outbreaks (bubble diameter constrained by the pore diameter) or under external shear flow, because $SiO_2(l)$ adheres strongly to a highly porous $ZrO_2(c)$ skeleton by capillary forces across a large contact area. In short, the dynamical view is that the $ZrO_2(c)$ skeleton helps to collect and retain the silica-rich liquid, playing an important *mechanical* role.

There is also a "steady-state" explanation (Fig. 2(b)), beginning with the interpretation of volatility diagrams.[24,25] Volatility diagrams represent chemical equilibria when *assuming* some volatile gas species are *in contact* with certain condensed phases—solid or liquid. Solid or liquid makes a difference here, because a liquid could flow in or flow out, easily retreating from a region if necessary. If a certain condensed phase retreats, then an originally high volatile gas pressure—assuming the condensed phase was there—loses its significance. For instance, pB_2O_3 in Fig. 11 of Opeka *et al.*[2] must appear more important than it really is in ZrB_2+SiC oxidation, because we know there is no $B_2O_3(l)$ to make contact with in reality at these temperatures. Another way of seeing this is that in reality all condensed-phase B_2O_3, if they exist, are solvated inside $SiO_2(l)$, with much lower activity than in pure $B_2O_3(l)$, and thus the actual pB_2O_3 vapor pressure should be lowered in proportion and will not be as dangerously high as it originally looks. This understanding of the volatility diagram may be translated into the following rule: *liquid phases will retreat from the region where some volatile gas species, were they in contact, will have high vapor pressure (approaching hydrostatic pressure inside the liquid), to region of lower vapor pressure according to the volatility diagram; after the retreat, the actual vapor pressure of the volatile gas species will*

be automatically lowered than what the volatility diagram has originally indicated for the evacuated region.

The above rule comes from thermochemistry. Applying the rule to oxidizing monolithic SiC above T_B (see Fig. 2(b) middle), we see that the only thermochemically sound steady-state arrangement is for $SiO_2(l)$ to retreat to the low pSiO–high pO_2 region, and let gas-phase diffusion take over in the intervening gap, where there will be no condensed liquid phase, thus shutting down the high gas volatility. Unfortunately, although this setup is thermochemically and diffusion-kinetically sound, it is obviously mechanically unstable. The "scale" would easily shear off or spall. This is fundamentally because in monolithic SiC, with only a single condensed-phase oxide product, which is a liquid, there is no way to satisfy both thermochemical and mechanical stabilities simultaneously at $T > T_B$.

In contrast, when oxidizing ZrB_2+SiC, one gets *two* condensed-phase oxide products. $ZrO_2(c)$ itself has only low volatilities of $ZrO(g)$ and $ZrO_2(g)$ (see Fig. 11 of Opeka *et al.*[2]). Furthermore it is a solid. So it does not retreat from the high SiO volatility region, maintaining mechanical connection with the main body. The silica-rich borosilicate liquid duly retreats from the high SiO volatility region, thereby removing the high SiO volatility automatically. This staggered placement of solid and liquid phases at $T > T_B$, with internal gas finger diffusion and gas–solid reactions (Fig. 2(b) bottom), is both thermochemically and mechanically sound if the $ZrO_2(c)$ skeleton is long enough, such that even after the retreat the liquid phase can still hold onto the solid by capillary forces, to have a "solid pillars, liquid roof" architecture as suggested by many experiments.[15,16,21,22] The actual oxidation of SiC particles at $T > T_B$ then no longer follows reaction (2), but directly

$$SiC(c) + O_2(g) \rightarrow SiO(g) + CO(g) \tag{4}$$

a gas–solid reaction without going through the liquid phase,[22] which will lead to a porous "SiC-depleted" substrate layer in the ZrB_2+SiC.[13] The $ZrO_2(c)$ "solid pillars" will also grow longer at the base by gas–solid reaction, with $O_2(g)$ reactant and $B_XO_Y(g)$ product. On the other end of the gas finger, we will have the reverse of reaction (3):

$$2SiO(g) + O_2 \rightarrow 2SiO_2(l) \tag{5}$$

which replenishes the "liquid roof".

The above explanation, if correct, could rationalize why the microstructure of ZrB_2+SiC is important for its oxidation resistance,[20] because the pore sizes of $ZrO_2(c)$ might be related to the preoxidation SiC particle sizes. As Gasch *et al.* mentioned,[13] "at 20 volume percent SiC, if the SiC particles are assumed to be small spheres randomly distributed throughout the HfB_2 matrix, the amount of SiC should be above the percolation threshold. This means that the SiC particles form a network that is interconnected in three dimensions." For a certain fixed volume fraction, smaller pores and better connectivity inside $ZrO_2(c)$ could enhance the collection and retention of the silica-rich liquid. Thus, nanoscale SiC particles might improve the oxidation resistance of ZrB_2+SiC,[20] by refining the microstructure of the *in situ* formed $ZrO_2(c)$ skeleton.

The proposed view also explains why 70–80 vol% of the composite is dedicated to ZrB_2. It is seen that a *porous* ZrO_2 could be advantageous for the oxidation resistance for a *mechanical* reason (not a diffusion kinetics one), if there is also a liquid oxide product phase to "collaborate" with. The porous skeleton needs to be strong enough as well as sufficiently long, to have enough room for the liquid oxide phase to retreat outward. Otherwise, the two phases may still have to separate ("high volatility blows away the liquid roof"), and the entire system would lose oxidation protection. One cannot have too much SiC (and thus the liquid) and not enough oxide skeleton, and maintain the mechanical and thermochemical stabilities of the "solid pillars, liquid roof" architecture. Because capillary force holds the solid and liquid phases together, microstructural refinement of the oxide scale will lead to stronger capillary adhesion per unit volume, which could lead to significant improvement of the overall oxidation resistance.

III. Oxygen Transport in Silica-Rich Liquid

From Section II model, we see that if $ZrO_2(c)$ has a percolating-holes microstructure, the borosilicate liquid will define the effective barrier against oxygen, irrespective of whether fully dense ZrO_2 is intrinsically better barrier (in open-circuit condition) against oxygen or not than the borosilicate liquid, as the liquid occupies both serial and parallel oxygen transport pathways in the "solid pillars, liquid roof" architecture. In this section we focus on the atomic-level events that govern oxygen transport in the borosilicate liquid.

Experimentally, it is still challenging to accurately determine the composition profile of the borosilicate liquid because boron is a light element. According to the Hertz–Knudsen–Langmuir equation,[32] the net evaporation flux of a species from a liquid surface is

$$J = \alpha \Delta p / (2\pi m k_B T)^{1/2} \tag{6}$$

Where Δp is the difference between the equilibrium vapor pressure and the actual vapor pressure of the species at the surface, and α is a coefficient of order 1. Because pure $B_2O_3(l)$ has much higher equilibrium vapor pressure than pure $SiO_2(l)$ in an oxygen-rich environment, a borosilicate liquid facing air would preferentially evaporate B_2O_3 instead of SiO_2. Thus the borosilicate liquid should be overall silica rich, with a composition gradient that is B_2O_3 depleted at the liquid–air interface, and B_2O_3 enriched at the gas finger–liquid interface (Fig. 2(b)), as $B_2O_3(g)$ and other boron-bearing gas species[31] are carried along with $SiO(g)$ in the gas finger and get absorbed into the liquid. Previously, Bongiorno and Pasquarello have studied oxygen transport in pure silica glass[28,33,34] using a multiscale modeling approach that combines high-level quantum mechanical (DFT) calculations of the diffusing oxygen species and local energy barriers, with kinetic Monte Carlo sampling of connected migration pathways. To bound the results, we decide to model a borosilicate liquid composition of equal B_2O_3 and SiO_2 proportions.

One major challenge in modeling any glass or liquid is to have reliable atomic structures. We have adopted the structure generation approach of Van Ginhoven, Jonsson, and Corrales,[35] which was shown to reproduce experimental pair distribution functions for pure silica. The approach requires a classical interatomic potential to perform long-time molecular dynamics (MD) simulations at the beginning, followed by further DFT optimizations. To generate the classical potential, we adopt the van Beest, Kramer, and van Santen parameterization[36] for Si–O interactions, but fit B–O and Si–B interactions to a series of small DFT calculations for bulk B_2O_3, using the software package GULP.[37] Then, starting from random positions for oxygen, boron and silicon atoms in the supercell, we perform a sequence of classical MD simulations at temperatures 6000, 5000, 4000, 3000, 2000, and 1000 K. The resulting structures were then used as input geometries for further DFT calculations (Vienna *ab initio* simulation program[38,39] with spin-polarized PW91 functional,[40] projector augmented wave method,[41,42] planewave kinetic energy cutoff 400 eV). For our initial studies, a cubic supercell containing $14SiO_2+7B_2O_3$ formula units is used, with total 77 atoms. The average density is 2.3 g/cm^3. A typical liquid structure at $T = 2500°C$, after further equilibration by *ab initio* MD, is shown in Fig. 3(a). It clearly has a framework structure with no long-range order, and contains with no dangling bonds (all Si are fourfold coordinated to O, and all B are threefold coordinated to O).

Based on these atomic structures, we have studied the thermodynamic stability and diffusion kinetics of solvated oxygen molecules O_2^* and atomic O^* in borosilicate liquid. The former stay inside the open cages of the framework and do not interact

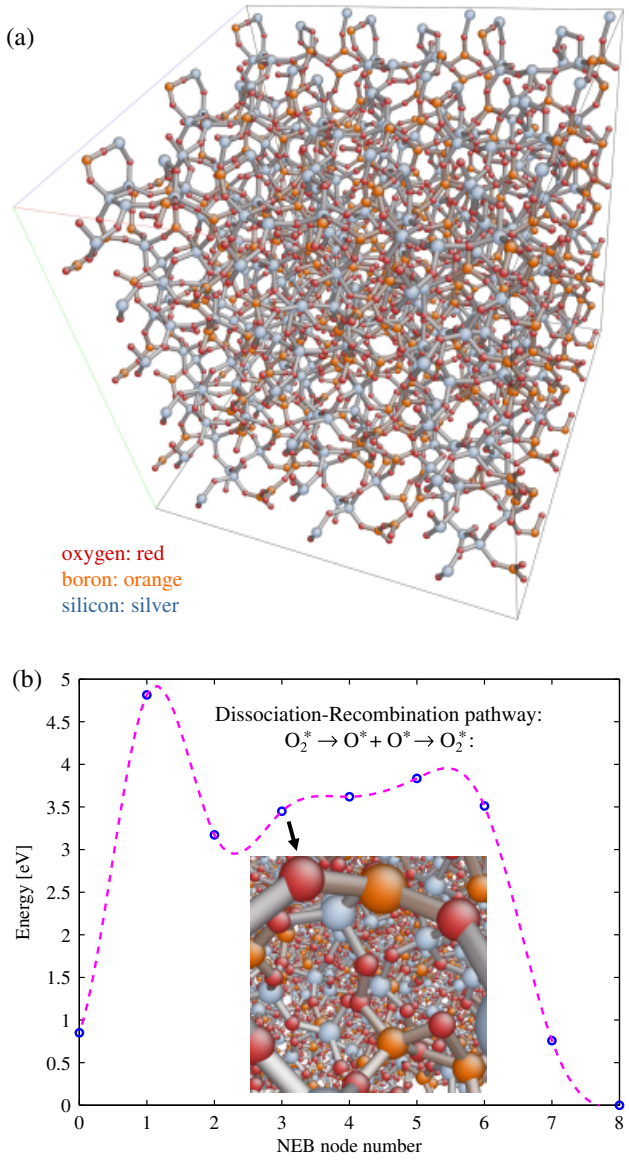

Fig. 3. (a) A typical borosilicate liquid structure ($14SiO_2+7B_2O_3$, plus one solvated O_2^*) generated from a sequence of long-time classical molecular dynamics simulations, followed by density functional theory (DFT) molecular dynamics simulation at 2500°C. Note that the supercell has been replicated three times in all three dimensions to facilitate visualization of the framework. (b) A typical DFT calculated minimum energy path (MEP) of dissociation–migration–recombination reaction inside the borosilicate framework: $O_2^* \rightarrow 2O^* \rightarrow O_2^*$, where oxygen exchange between O_2^* and the network occurs. The inset shows the atomic configuration (replicated for visualization) of node 3 on the MEP, which contains one peroxyl linkage (Si–O–O–B) and one extra B–O–B bridge. Oxygen: red, boron: orange, silicon: silver.

chemically with the framework. The latter are chemically incorporated into the network in the form of peroxyl linkage Si–O–O–B[27,28] (Fig. 3(b) inset), extra bridging O between two B (Fig. 3(b) inset), and others. Because diffusion could be a rare event, simply performing MD simulations and tracking the mean squared displacements may not be sufficient, and energy-landscape exploration techniques such as nudged elastic band (NEB)[43] calculations may be needed. These methods compute the minimum energy path (MEP) and saddle-point configuration of thermally activated processes, and then use transition-state theory[44] to estimate the rates.

First, we place one O_2^* inside a cage and perform DFT MD simulation at 2500°C for 11 ps (see movie S1 at http://alum.mit.edu/www/liju99/Papers/08/JACerS/). It is very clear from the MD trajectory (in contrast to those of simple liquids such as Ar, as well as water) that the borosilicate liquid still maintains a very "rigid" framework at 2500°C. Indeed, pure silica is a strong glass-forming liquid,[45] and its viscosity does not show a precipitous drop above the glass transition temperature. For instance, even at 2500°C, pure silica still has a shear viscosity $\eta \sim 10^4$ poise, which is a million times thicker than that of room-temperature water. This means the liquid still has a well-defined network structure at any given moment, and its topological change does not occur at the same timescale as, for instance, its own Si–O–Si bond stretching. Also, from the 11 ps *ab initio* MD trajectory, we find the O_2^* is essentially trapped inside one cage. It just bounces back and forth many times inside a jiggling cage, with no possibility of escape within the MD simulation timescale. These facts suggest that one is still justified to use transition-state theory and numerical schemes like the NEB method[43] to characterize diffusion of O_2^*, despite it is embedded in a *liquid*. From our MD simulations, adding 50% B_2O_3 to silica does not seem to change this consideration qualitatively.

A complication for the NEB calculation is that unlike in crystals, diffusion inside an amorphous framework has a distribution of local minima and activation energies.[33,34] Not all cages have the same volume, nor the same energy for opening up the constrictions (see movie S2) when O_2^* squeezes from one cage into the other. In Fig. 5 of Bongiorno *et al.*,[33] we have shown a typical DFT–NEB-calculated MEP of O_2^* diffusion (vehicular diffusion mode). The forward hop barrier is 1.8 eV, whereas the backward hop barrier is 1.4 eV. These are somewhat higher than the 1.12 eV effective migration barrier that Bongiorno and Pasquarello[34] predicted for O_2^* vehicular diffusion in pure silica, perhaps because of the B_2O_3 modifications to the network. More calculations are needed in order to have better statistics.

For vehicular diffusion inside a liquid, there is a well-known Stokes–Einstein relation:

$$D(O_2^*) \sim k_B T / 6\pi\eta R(O_2^*) \tag{7}$$

where $R(O_2^*)$ is a nominal hydrodynamic radius of the molecule. Even though the Stokes–Einstein relation is quite successful in simple liquids, it can fail in network-forming liquids.[46,47] Norton measured the permeation of gaseous oxygen through vitreous silica and found an activation energy of 27 kcal/mol (1.17 eV)[48] for $D(O_2^*)$, in substantial agreement with later measurements.[26] However, the activation energy governing η, the viscosity of vitreous silica, is in the range of 5.3–7.5 eV.[49] So clearly Eq. (7) does not work. From our DFT modeling, the physics governing the activation energy of O_2^* vehicular diffusion is seen to be an *elastic* deformation of the framework (elastic opening of the constrictions, see movie S2) without changing its network topology. But the physics behind the activation energy of η must involve network topology changes, which necessarily involve Si–O bond breaking.

In addition to O_2^* vehicular diffusion, oxygen transport may also occur by Grotthuss-type oxygen-hopping mechanisms,[50] mediated by network defects such as peroxyl linkage[27,28] or oxygen-deficient centers.[29,30] These mechanisms would involve bond breaking, and typically higher effective activation energies—mostly due to the formation energies of such defects. Figure 3(b) shows one such pathway, where an O_2^* breaks up into two O^*:

$$O_2^* \rightarrow O^* + O^* \tag{8}$$

The two O^*s then move independently of each other for a while, and eventually recombine on the other side of the cage (see movie S3) in this particular NEB calculation setup. In node 3 of the calculated MEP (Fig. 3(b) inset), one O^* takes the form of a peroxyl linkage Si–O–O–B, while the other O^* takes the form of an additional B–O–B bridge, making the two boron atoms four-fold coordinated.

We find from multiple NEB calculations in the borosilicate framework that these coordination defects, once formed, can interconvert easily, suggesting low migration barriers, similar to

interstitial defects in metals. On average, the right-hand side (RHS) of reaction (8) is about 2.8 eV higher in potential energy than the left-hand side (LHS), as indicated by node 3, 4, 5, 6 of Fig. 3(b) MEP (see also movie S3). However, there are two free translational centers on the RHS: the two O*s, once formed, can move independently of each other inside the liquid. The LHS has only one free translational center, in order to maintain its molecular form. Thus the RHS of reaction (8) has entropic advantage of approximately $k_B \ln c$, where c is the prevalent oxygen carrier concentration (per formula unit of SiO_2+B_2O_3), whereas the LHS has energy advantage. The classic enthalpy–entropy tradeoff in free energy then suggests that there exists a temperature T_C, below which O_2^* is dominant in concentration, and above which O*s are dominant, if the borosilicate is in an oxygen-rich environment (the equivalent pO_2 is high). In lower equivalent pO_2 environment, oxygen-deficient centers[29,30] are also possible carriers.

In reference to O_2 in the gas phase, we find the average potential energy of O_2^* solvated in borosilicate is 0.73 eV per molecule, which is essentially the elastic energy in the framework needed to accommodate the molecule. The average potential energy of O*, on the other hand, is about 1.78 eV per O. These energies are used to compute the concentration of O_2^* and O* in borosilicate in equilibration with $pO_2 = 0.1$ atm, shown in Fig. 4. Note that $c_{O_2^*}$ scales linearly with pO_2, whereas c_{O^*} scales linearly with $(pO_2)^{1/2}$. Thus, deeper and deeper into the scale, as the oxygen chemical potential gets lower and lower, the Grotthuss-type oxygen transport should become relatively more and more important.

Norton measured the solubility of O_2^* in pure silica at 1078°C and $pO_2 = 1$ atm to be 1.9×10^{-3} cm^3 STP O_2 gas per cm^3 silica.[48] This amounts to 5.1×10^{16} per cm^3 silica or a dimensionless concentration of about $c = 10^{-5}$, at $pO_2 = 1$ atm. This is about two orders of magnitude higher than our DFT-predicted O_2^* solubility in borosilicate, shown in Fig. 4. This could be due to the structural difference between pure silica framework and borosilicate framework. As Bongiorno and Pasquarello[34] noted, the potential energy of O_2^* depends sensitively on the cage interstice volume, and there is certainly a structural difference between pure silica and B_2O_3-modified networks. This could also be partly due to the intrinsic errors of PW91 density functional,[40] which are known to give large errors treating isolated molecules (the reference state), and nonbonding interactions (O_2^* interactions with the framework).

The above uncertainties aside, it is still a rather conservative estimate that above $T_C \sim 1500$°C the dominant oxygen carriers in the borosilicate "liquid roof" are network defects instead of molecular O_2^*, because there are other factors not shown in Fig. 4 that disfavors the Deal–Grove mechanism: (a) the DFT calculations indicate that the O*s not only have entropy advantage, but also mobility advantages over O_2^*, (b) intense aerothermal heating environment may introduce a significant level of dissociated oxygen on the outer liquid surface,[14,33] which would favor O* diffusion from a nonequilibrium kinetics perspective, (c) as pO_2 drops from $\sim 10^4$ Pa on the outer liquid surface to $< 10^{-5}$ Pa equivalent at the internal gas finger–liquid interface (Fig. 2(b)) according to the volatility diagram,[2,21] the balance will shift more and more away from O_2^* vehicular diffusion to network defect Grotthuss diffusion. Oxygen-deficient centers[29,30] may play a significant role in oxygen transport at low equivalent pO_2s. It seems plausible that oxygen in the borosilicate liquid could react with the underlying substrate or SiO(g), injecting oxygen vacancies (e.g., regions of high B and Si stoichiometry) into the liquid, which then diffuse up the scale to recombine with O_2^* or O* somewhere inside the liquid. (d) In all the DFT calculations, we have only considered neutral network defects. Charging the defects may significantly greatly reduce their formation energies,[30,51] although we will then need to solve the complementary problem of what other defects compensate the charge and carry out ambipolar diffusion under open-circuit condition.

The mobility advantage of the peroxyl linkage over O_2^* suggests that arc-jet testing,[13,33] which introduces a nonequilibrium distribution of dissociated oxygen atoms on the surface, will likely lead to faster oxidation than ordinary furnace testing at the same temperature. Also, because the network defects are chemically incorporated into the network and thus interact more strongly with solutes than O_2^*, small changes in the glass chemistry could lead to large changes in the oxygen diffusivity by defect trapping/gettering,[30] much more than what Eq. (7) could have suggested.

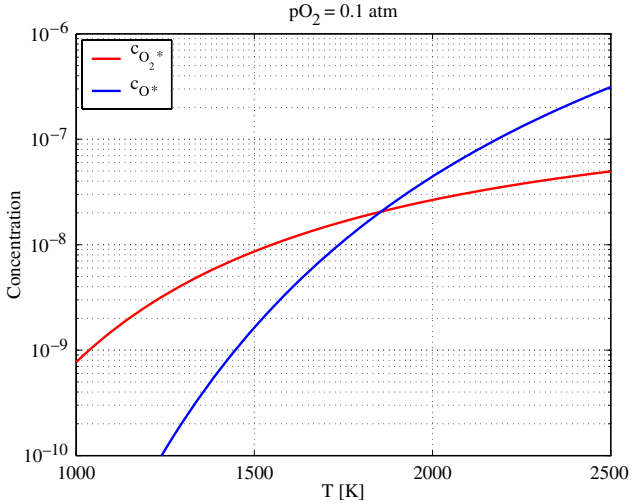

Fig. 4. Estimated concentrations of O_2^* and O* (per formula unit of SiO_2+B_2O_3) inside borosilicate framework, in equilibration with $pO_2 = 0.1$ atm.

IV. Summary

We present a congruent explanation of the oxidation protection of ZrB_2+SiC based on a "solid pillars, liquid roof" scale architecture, where the borosilicate liquid defines the effective diffusion barrier, and the solid zirconia collects and retains the liquid and provides mechanical support. Internal gas fingers will form as the liquid phase retreats to remove the high SiO volatility above a boiling transition temperature. At such high temperatures, to satisfy both thermochemical and mechanical stabilities, the "solid pillars, liquid roof" architecture seems to be a viable solution, not available to monolithic SiC.

Compared with the borosilicate liquid phase, whether fully dense zirconia is blocking or unblocking to oxygen in open-circuit condition depends on its electronic conductivity (transference number), which in turn depends on how the charge defects are compensated inside the crystal, related to the amount of impurities. If the zirconia phase has a highly porous microstructure, however, then the above discussion is likely irrelevant and the borosilicate liquid phase will control the effective diffusion barrier, because it will occupy both serial and parallel oxygen transport pathways.

At low temperatures, it is commonly accepted that molecular oxygen O_2^* dominates oxygen transport. However, from first-principles calculations with detailed borosilicate atomic structures, it seems unlikely that this will remain the case at temperatures of practical interest for the ZrB_2+SiC thermal protection system (above 1500°C). This means that the oxidation rate will likely have a complex, sublinear dependence with respect to the external oxygen partial pressure. Also, if the oxygen carriers are chemically incorporated and interact strongly with the framework, there is hope that by tuning the glass composition, the carriers could be trapped, thereby slowing down oxygen diffusion.

Acknowledgments

We would like to thank Mark Opeka, Inna Talmy, Robert Rapp, Triplicane Parthasarathy, Ronald Kerans, and Nitin Padture for instructive discussions.

References

[1]W. G. Fahrenholtz, G. E. Hilmas, I. G. Talmy, and J. A. Zaykoski, "Refractory Diborides of Zirconium and Hafnium," *J. Am. Ceram. Soc.*, **90** [5] 1347–64 (2007).

[2]M. M. Opeka, I. G. Talmy, and J. A. Zaykoski, "Oxidation-Based Materials Selection for 2000 Degrees C Plus Hypersonic Aerosurfaces: Theoretical Considerations and Historical Experience," *J. Mater. Sci.*, **39** [19] 5887–904 (2004).

[3]A. K. Kuriakose and J. L. Margrave, "The Oxidation Kinetics of Zirconium Diboride and Zirconium Carbide at High Temperatures," *J. Electrochem. Soc.*, **111** [7] 827–31 (1964).

[4]J. B. Berkowitz-Mattuck, "High-Temperature Oxidation .3. Zirconium and Hafnium Diborides," *J. Electrochem. Soc.*, **113** [9] 908–14 (1966).

[5]L. Kaufman, E. V. Clougherty, and J. B. Berkowitz-Mattuck, "Oxidation Characteristics of Hafnium and Zirconium Diboride," *Trans. Metall. Soc. AIME*, **239** [4] 458–66 (1967).

[6]R. J. Irving and I. G. Worsley, "Oxidation of Titanium Diboride and Zirconium Diboride at High Temperatures," *J. Less-Common Met.*, **16** [2] 103–12 (1968).

[7]E. V. Clougherty, R. L. Pober, and L. Kaufman, "Synthesis of Oxidation Resistant Metal Diboride Composites," *Trans. Metall. Soc. AIME*, **242** [6] 1077–82 (1968).

[8]W. C. Tripp and H. C. Graham, "Thermogravimetric Study of Oxidation of ZrB_2 in Temperature Range of 800 Degrees to 1500 Degrees," *J. Electrochem. Soc.*, **118** [7] 1195–9 (1971).

[9]W. C. Tripp, H. H. Davis, and H. C. Graham, "Effect of an SiC Addition on Oxidation of ZrB_2," *Am. Ceram. Soc. Bull.*, **52** [8] 612–6 (1973).

[10]J. W. Hinze, W. C. Tripp, and H. C. Graham, "The High-Temperature Oxidation Behavior of a HfB_2+20 v/o SiC Composite," *J. Electrochem. Soc.*, **122** [9] 1249–54 (1975).

[11]M. M. Opeka, I. G. Talmy, E. J. Wuchina, J. A. Zaykoski, and S. J. Causey, "Mechanical, Thermal, and Oxidation Properties of Refractory Hafnium and Zirconium Compounds," *J. Eur. Ceram. Soc.*, **19** [13–14] 2405–14 (1999).

[12]F. Monteverde and A. Bellosi, "Oxidation of ZrB_2-Based Ceramics in Dry Air," *J. Electrochem. Soc.*, **150** [11] B552–9 (2003).

[13]M. Gasch, D. Ellerby, E. Irby, S. Beckman, M. Gusman, and S. Johnson, "Processing, Properties and Arc Jet Oxidation of Hafnium Diboride/Silicon Carbide Ultra High Temperature Ceramics," *J. Mater. Sci.*, **39** [19] 5925–37 (2004).

[14]J. Marschall, A. Chamberlain, D. Crunkleton, and B. Rogers, "Catalytic Atom Recombination on ZrB_2/SiC and HfB_2/SiC Ultrahigh-Temperature Ceramic Composites," *J. Spacecraft Rockets*, **41** [4] 576–81 (2004).

[15]E. Opila, S. Levine, and J. Lorincz, "Oxidation of ZrB_2- and HfB_2-Based Ultra-High Temperature Ceramics: Effect of Ta Additions," *J. Mater. Sci.*, **39** [19] 5969–77 (2004).

[16]A. Chamberlain, W. Fahrenholtz, G. Hilmas, and D. Ellerby, "Oxidation of ZrB_2-SiC Ceramics Under Atmospheric and Reentry Conditions," *Refract. Appl. Trans.*, **1** [2] 2–8 (2005).

[17]W. G. Fahrenholtz, "The ZrB_2 Volatility Diagram," *J. Am. Ceram. Soc.*, **88** [12] 3509–12 (2005).

[18]A. Rezaie, W. G. Fahrenholtz, and G. E. Hilmas, "Oxidation of Zirconium Diboride-Silicon Carbide at 1500 Degrees C at a Low Partial Pressure of Oxygen," *J. Am. Ceram. Soc.*, **89** [10] 3240–5 (2006).

[19]I. G. Talmy, J. A. Zaykoski, M. M. Opeka, and A. H. Smith, "Properties of Ceramics in the System ZrB_2-Ta_5Si_3," *J. Mater. Res.*, **21** [10] 2593–9 (2006).

[20]S. S. Hwang, A. L. Vasiliev, and N. P. Padture, "Improved Processing, and Oxidation-Resistance of ZrB_2 Ultra-High Temperature Ceramics Containing SiC Nanodispersoids," *Mater. Sci. Eng. A*, **464** [1–2] 216–24 (2007).

[21]W. G. Fahrenholtz, "Thermodynamic Analysis of ZrB_2-SiC Oxidation: Formation of a SiC-Depleted Region," *J. Am. Ceram. Soc.*, **90** [1] 143–8 (2007).

[22]A. Rezaie, W. G. Fahrenholtz, and G. E. Hilmas, "Evolution of Structure During the Oxidation of Zirconium Diboride-Silicon Carbide in Air up to 1500 Degrees C," *J. Eur. Ceram. Soc.*, **27** [6] 2495–501 (2007).

[23]T. A. Parthasarathy, R. A. Rapp, M. M. Opeka, and R. J. Kerans, "A Model for the Oxidation of ZrB_2, HfB_2 and TiB_2," *Acta Mater.*, **55** [17] 5999–6010 (2007).

[24]A. H. Heuer and V. L. K. Lou, "Volatility Diagrams for Silica, Silicon-Nitride, and Silicon-Carbide and Their Application to High-Temperature Decomposition and Oxidation," *J. Am. Ceram. Soc.*, **73** [10] 2789–803 (1990).

[25]V. L. K. Lou, T. E. Mitchell, and A. H. Heuer, "Graphical Displays of the Thermodynamics of High-Temperature Gas–Solid Reactions and Their Application to Oxidation of Metals and Evaporation of Oxides," *J. Am. Ceram. Soc.*, **68** [2] 49–58 (1985).

[26]B. E. Deal and A. S. Grove, "General Relationship for Thermal Oxidation of Silicon," *J. Appl. Phys.*, **36** [12] 3770–8 (1965).

[27]A. Bongiorno and A. Pasquarello, "Oxygen Species in SiO_2: A First-Principles Investigation," *Microelectron. Eng.*, **59** [1–4] 167–72 (2001).

[28]A. Bongiorno and A. Pasquarello, "Oxygen Diffusion Through the Disordered Oxide Network During Silicon Oxidation," *Phys. Rev. Lett.*, **88** [12] 125901 (2002).

[29]V. B. Sulimov and V. O. Sokolov, "Cluster Modeling of the Neutral Oxygen Vacancy in Pure Silicon Dioxide," *J. Non-Cryst. Solids*, **191** [3] 260–80 (1995).

[30]P. E. Blochl, "First-Principles Calculations of Defects in Oxygen-Deficient Silica Exposed to Hydrogen," *Phys. Rev. B*, **62** [10] 6158–79 (2000).

[31]A. W. Weimer, W. G. Moore, R. P. Roach, J. E. Hitt, R. S. Dixit, and S. E. Pratsinis, "Kinetics of Carbothermal Reduction Synthesis of Boron-Carbide," *J. Am. Ceram. Soc.*, **75** [9] 2509–14 (1992).

[32]J. P. Hirth and G. M. Pound, "Coefficients of Condensation, Evaporation and Thermal Accommodation," *Prog. Mater. Sci.*, **11** [1] 1–190 (1963).

[33]A. Bongiorno, C. J. Forst, R. K. Kalia, J. Li, J. Marschall, A. Nakano, M. M. Opeka, I. G. Talmy, P. Vashishta, and S. Yip, "A Perspective on Modeling Materials in Extreme Environments: Oxidation of Ultrahigh-Temperature Ceramics," *MRS Bull.*, **31** [5] 410–8 (2006).

[34]A. Bongiorno and A. Pasquarello, "Multiscale Modeling of Oxygen Diffusion Through the Oxide During Silicon Oxidation," *Phys. Rev. B*, **70** [19] 195312 (2004).

[35]R. M. Van Ginhoven, H. Jonsson, and L. R. Corrales, "Silica Glass Structure Generation for Ab Initio Calculations Using Small Samples of Amorphous Silica," *Phys. Rev. B*, **71** [2] 024208 (2005).

[36]B. W. H. Van Beest, G. J. Kramer, and R. A. Van Santen, "Force-Fields for Silicas and Aluminophosphates Based on Abinitio Calculations," *Phys. Rev. Lett.*, **64** [16] 1955–8 (1990).

[37]J. D. Gale and A. L. Rohl, "The General Utility Lattice Program (GULP)," *Mol. Simulation*, **29** [5] 291–341 (2003).

[38]G. Kresse and J. Hafner, "Ab-Initio Molecular-Dynamics Simulation of the Liquid-Metal Amorphous-Semiconductor Transition in Germanium," *Phys. Rev. B*, **49** [20] 14251–69 (1994).

[39]G. Kresse and J. Furthmuller, "Efficient Iterative Schemes for Ab Initio Total-Energy Calculations Using a Plane-Wave Basis Set," *Phys. Rev. B*, **54** [16] 11169–86 (1996).

[40]J. P. Perdew, J. A. Chevary, S. H. Vosko, K. A. Jackson, M. R. Pederson, D. J. Singh, and C. Fiolhais, "Atoms, Molecules, Solids, and Surfaces—Applications of the Generalized Gradient Approximation for Exchange and Correlation," *Phys. Rev. B*, **46** [11] 6671–87 (1992).

[41]P. E. Blochl, "Projector Augmented-Wave Method," *Phys. Rev. B*, **50** [24] 17953–79 (1994).

[42]G. Kresse and D. Joubert, "From Ultrasoft Pseudopotentials to the Projector Augmented-Wave Method," *Phys. Rev. B*, **59** [3] 1758–75 (1999).

[43]G. Henkelman and H. Jonsson, "Improved Tangent Estimate in the Nudged Elastic Band Method for Finding Minimum Energy Paths and Saddle Points," *J. Chem. Phys.*, **113** [22] 9978–85 (2000).

[44]G. Mills, H. Jonsson, and G. K. Schenter, "Reversible Work Transition-State Theory—Application to Dissociative Adsorption of Hydrogen," *Surf. Sci.*, **324** [2–3] 305–37 (1995).

[45]C. A. Angell, "Formation of Glasses from Liquids and Biopolymers," *Science*, **267** [5206] 1924–35 (1995).

[46]F. H. Stillinger, "A Topographic View of Supercooled Liquids and Glass-Formation," *Science*, **267** [5206] 1935–9 (1995).

[47]S. H. Chen, F. Mallamace, C. Y. Mou, M. Broccio, C. Corsaro, A. Faraone, and L. Liu, "The Violation of the Stokes-Einstein relation in Supercooled Water," *Proc. Ntl. Acad. Sci. USA*, **103** [35] 12974–8 (2006).

[48]F. J. Norton, "Permeation of Gaseous Oxygen through Vitreous Silica," *Nature*, **191** [478] 701 (1961).

[49]R. H. Doremus, "Viscosity of Silica," *J. Appl. Phys.*, **92** [12] 7619–29 (2002).

[50]N. Agmon, "The Grotthuss Mechanism," *Chem. Phys. Lett.*, **244** [5–6] 456–62 (1995).

[51]C. G. Van de Walle and J. Neugebauer, "Universal Alignment of Hydrogen Levels in Semiconductors, Insulators and Solutions," *Nature*, **423** [6940] 626–8 (2003). □